ACS APPLIED MATERIALS & INTERFACES

Research Article

www.acsami.org

Extension of Light-Harvesting Area of Bulk-Heterojunction Solar Cells by Cosensitization with Ring-Expanded Metallophthalocyanines Fused with Fluorene Skeletons

Satoshi Yamamoto and Mutsumi Kimura*

Division of Chemistry and Materials, Faculty of Textile Science and Technology, Shinshu University, Ueda 386-8567, Japan

ABSTRACT: Near-IR absorbing zinc fluorenocyanine complexes **1**−**3** were designed and synthesized as a cosensitizer for bulk-heterojunction solar cells. Fusing fluorene rings with the porphyrazine rings resulted in narrower band gap and stabilization of both the HOMO and LUMO energy levels compared with a zinc phthalocyanine complex. The synthesized fluorenocyanines **1**−**3** were incorporated into bulk-heterojunction solar cells based on regioregular poly(3-hexylthiophene) and 1-(3-methoxycarbonyl)-propyl-1-phenyl-(6,6)C_{61}. The addition of **3** decorated with eight alkyl chains resulted in improved device performance with a 16% enhancement of the short circuit current compared with that of the reference cell without **3**.

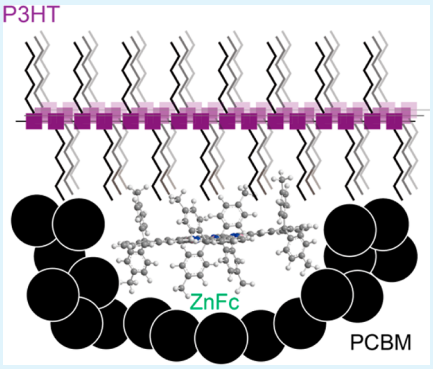

KEYWORDS: *phthalocyanine, fluorene, band gap, HOMO and LUMO, solar cells, bulk heterojunction*

INTRODUCTION

Organic photovoltaic devices (OPVs) based on thin films of organic semiconductors have been intensely investigated as a promising candidate for low-cost, lightweight, and scalable solar cells.[1−3] The performance of OPVs was greatly improved by producing an interpenetrating nanostructured interface between donor and acceptor materials to overcome the limited diffusion length of excitons in organic semiconductors. A bulk heterojunction (BHJ) architecture, which is constructed through a spontaneous phase-separation of highly soluble donor and acceptor materials, provides a suitable nanostructure for high conversion efficiencies of OPVs, as well as printable fabrication processes.[4] Controlling BHJ structure in the active layers allows a high interfacial area that optimizes the exciton dissociation and the efficient transport of the generated charges to the electrodes.[5,6] BHJ solar cells based on a blend of regioregular poly(3-hexylthiophene) (P3HT) and 1-(3-methoxycarbonyl)-propyl-1-phenyl-(6,6)C_{61} (PCBM) are a benchmark active layer with average power conversion efficiencies (PCE) of 2−4% under a standard global AM 1.5 illumination (100 mW/cm^2).[7−12] Since the light-harvesting area of P3HT is limited to a visible range less than 650 nm, a P3HT/PCBM active layer can not convert the energy of red light into electricity. To further enhance the performance of BHJ solar cells, several efforts have been devoted to the development of tandem architectures, novel active layer materials based on low band gap polymers, and additional cosensitizers.[3] Adding cosensitizers with energy levels that are intermediate of those of conjugated polymers and PCBM into the blended active layers is a simple and versatile approach, and several near-IR absorbing molecules have been used as a cosensitizer in BHJ solar cells to expand the light-harvesting region.[13−17]

Phthalocyanines (Pcs) and their metal complexes have been widely investigated as near-IR absorbing dyes because of their high stability, the presence of an intense absorption band in the near-IR region, and tunable redox activity.[18] Regarding BHJ solar cells, several groups have reported the enhancement of PCE values through the expansion of the light harvesting region of the cells by the addition of silicon phthalocyanine derivatives (SiPc), liquid crystalline Pcs, and fullerene-functionalized ZnPcs.[19−23] Ohkita et al. discussed the location of SiPc at the interface of P3HT and PCBM domains in the active layer of BHJ solar cells.[23] They found that the selective doping of SiPc at the disordered P3HT domains improved device performance. However, ZnPc lacking axial substituents did not exhibit the PCE improvement in the P3HT/PCBM-based BHJ solar cells. In this study, we developed near-IR absorbing cosensitizers based on ring-expanded ZnPcs for the BHJ solar cells.

The electronic structure and properties of MPcs can be tailored by modifying the macrocyclic ligands and changing the central metals.[24] Substitutions to the macrocycles by electron-donating and electron-accepting groups were found to change the electronic properties. Kobayashi et al. reported the significant red shift of the Q-band beyond 1000 nm in phosphorus phthalocyanines by the introduction of electron-donating groups at the α-positions and deformation of the

Received: February 14, 2013
Accepted: April 24, 2013
Published: April 24, 2013

   dx.doi.org/10.1021/am4005896 | ACS Appl. Mater. Interfaces 2013, 5, 4367−4373

planarity of the *Pc* plane.[25] The other approach to tuning the electronic properties of MPcs is to modify the extension of the π-conjugation system. Considerable studies were concerned with expanded MPcs that fuse additional aromatic rings attached to the *Pc* ring. Muranaka et al. succeeded in shifting the Q-band and stabilizing the LUMO level by fusing an electron-accepting azulene skeleton with the porphyrazine ring.[26] While fluorene rings have been used as molecular components for various organic devices,[27] a porphyrazine derivative fused with fluorene rings has not been reported. Fusing fluorene rings with the porphyrazine rings may change the electronic structure. Here, we describe the synthesis and characterization of zinc fluorenocyanines (ZnFcs) **1**−**3**, in which four fluorene rings were connected with the porphyrazine ring (Figure 1). We also discuss solar cell performance improved by the addition of ZnFcs in the blended films of P3HT and PCBM.

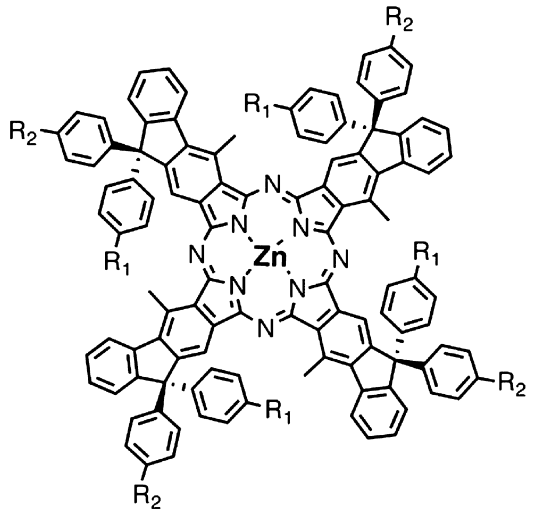

Figure 1. Structure of zinc fluorenocyanines **1**−**3**. ZnFcs **1**−**3** are composed of a mixture of structural isomers.

RESULTS AND DISCUSSION

Scheme 1 illustrates the synthetic route of ZnFcs **1**−**3**. Precursors **9**−**11** were synthesized from 4-bromo-2-methylaniline as a starting material through seven steps. The reaction of aniline with tetrabutylammonium tribromide in a CH_2Cl_2-methanol readily gave 3,4-dibromo-2-methylaniline.[28] After the conversion of amine to iodide,[29] a palladium-catalyzed coupling reaction between **4** and 2-(ethoxycarbonyl)phenylboronic acid pinacol ester gave **5**. The fluorenone derivative **6** was obtained in a good yield by treating **5** with concentrated sulfuric acid.[30] Two aryl Grignard reagents, *p*-TolMgBr and *p*-hexylphenyMgBr, were reacted with **6** in diethyl ether at reflux temperature.[31] The corresponding alcohol derivatives **7** and **8** were isolated in good yields. The Friedel−Crafts reactions of **7** and **8** with toluene or hexylbenzene were carried out in the presence of an excess amount of CF_3SO_3H to give three 9,9-diarylfluorenes. In the final step, the bromides were transformed into dinitriles **9**−**11** by treatment with CuCN in 1-methyl-2-pyrrolidone (NMP). The target ZnFcs **1**−**3** were prepared by tetracyclization of **12**−**15** by refluxing in 2-(dimethylamino)ethanol (DMAE) in the presence of Zn-$(AcO)_2$. All final ZnFcs and their corresponding intermediates were fully characterized by using spectroscopic techniques. ZnFcs **1**−**3** were obtained as a mixture of structural isomers depending on the direction of the fluorene rings.

The extended planar shape of nonsubstituted MPcs resulted in poor solubilities in any solvents owing to their strong tendency to form dense stacking through the intermolecular $\pi-\pi$ interaction. According to the molecular models of **1**−**3** (Figure 2a), aryl substituents at the C9 position of the fluorene in **1**−**3**, which lie out of the plane of the macrocycles, act as a steric hindrance to avoid the stacking among the macrocycles. Thus, ZnFcs **1**−**3** exhibited a good solubility in common organic solvents, such as toluene, $CHCl_3$, and THF. Figure 2b shows the UV−vis and fluorescence spectra of **3** in THF. ZnFc **3** exhibited a sharp peak at λ_{max} = 711 nm and a relatively weak peak at λ_{max} = 386 nm as the Q-band and the Soret band.[32] The position of the Q-band shifted to 33 nm compared with that of zinc(II) tetra(*tert*-butyl)phthalocyanine (Zn(*t*-Bu)*Pc*, λ_{max} = 678 nm). Since the Q-band can be assigned to a transition between the HOMO and the LUMO or LUMO + 1, the HOMO−LUMO band gap of **3** was slightly smaller than that of Zn(*t*-Bu)*Pc*. When **3** was excited at the Q-band of the ZnFc core in a degassed THF solution, it exhibited a strong fluorescence at 718 nm. The optical HOMO−LUMO band-gaps (E_g) for **1**−**3** were determined to be 1.7 eV from the cross point of the normalized absorption and fluorescence spectra. Figure 2c shows the UV−vis spectra of spin-coated films of **1**−**3** on quartz plates. The Q-band of the spin-coated film of **1** was broadened relative to that in THF, which implies the formation of aggregates in the solid films. In contrast, **3** possessing eight hexyl chains displayed a sharp Q-band and the half width of the Q-band in the solid film was almost the same as that in the solution. This indicates that the introduction of alkyl chains prevents the formation of aggregation in the solid films.

The onset potentials (E'_{ox}) for the first oxidation of **1**−**3** appeared at +0.53 V versus ferrocene/ferricenium redox couple (Fc/Fc^+) determined by cyclic voltammetry measurement in dry CH_2Cl_2 containing 0.1 M tetrabutylammonium perchlorate (TBAP) as a supporting electrolyte (Figure 3a).[33] The HOMO energy levels of **1**−**3** were estimated to be −5.3 eV from the E'_{ox} values calibrated by the Fc/Fc^+ redox couple versus vacuum.[34] The LUMO energy levels for **1**−**3**, estimated from the HOMO energy levels and E_g, were evaluated to be −3.6 eV. The ring expansion from phthalocyanine to naphthalocyanine (Nc) resulted in a decreasing HOMO−LUMO gap because of the destabilization of the HOMO energy level.[25,26] In contrast, the HOMO and LUMO energy levels of **1**−**3** were lower than those of Zn(*t*-Bu)*Pc* (HOMO = −5.0 eV, LUMO = −3.1 eV), indicating that the fusing of fluorene rings with the porphyrazine ring leads to the stabilization of HOMO and LUMO energy levels. The UV−vis spectra of the spin-coated films of **1**−**3** remained unaltered after being stored in air under ambient light for one month, revealing good stabilities of **1**−**3** under ambient conditions because of the stabilization of HOMO energy levels. Stability under ambient conditions is one of the most important factors for using molecules as optoelectronic materials in organic-based devices.

The energy levels of ZnFcs **1**−**3** are located at the intermediate between those of P3HT (HOMO = −5.1 eV,

Scheme 1. Syntheses of Zinc Fluorecyanines 1−3[a]

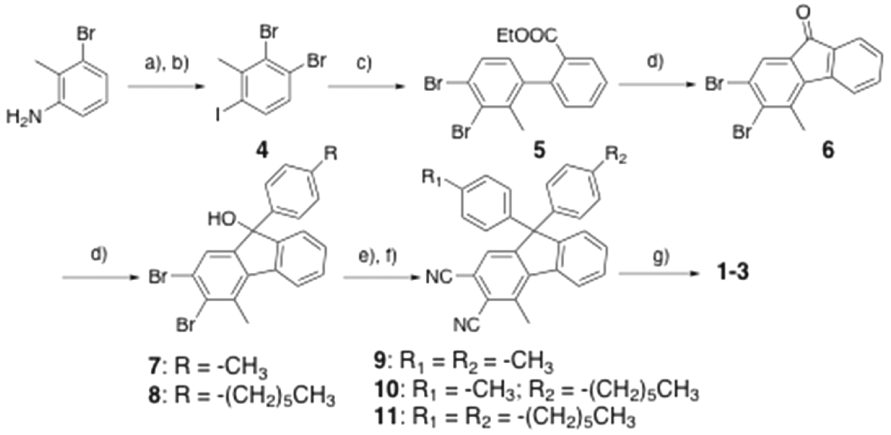

[a](a) TBA Br_3, CH_2Cl_2 MeOH; (b)HBF_4, NaNO, Kl; (c) 2 (ethoxycarbonyl)phenyiboronic acid pinacol ester, $Pd(PPh)_4$, toluene/THF/$NaCO_3$ aq; (d) H_2SO_4; (e) ArMgBr, Et_2O; (d) ArH, CF_3SO_3H; (f) CuCN, NMP; (g) Zn(AcO), DMAE.

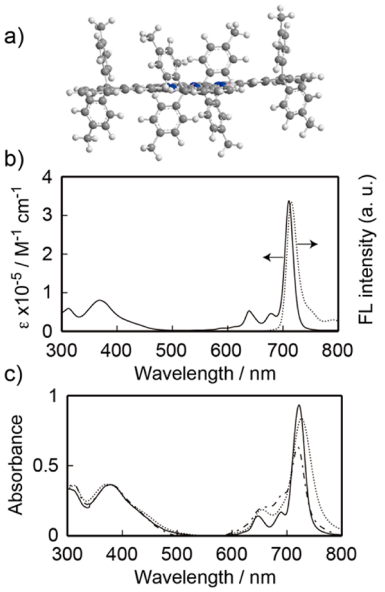

Figure 2. (a) Computer-simulated molecular structure of **1** optimized by Chem3D. (b) UV−vis and fluorescence spectra of **3** in THF. (c) UV−vis spectra of spin-coated thin films of **1**−**3** on quartz substrates: **1**, dashed line; **2**, dotted line; **3**, solid line.

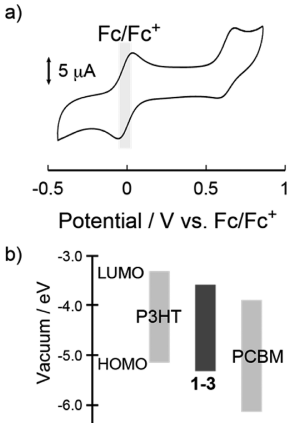

Figure 3. (a) Cyclic voltammetry data for **1** containing ferrocene as an internal standard. Cyclic voltammogram was acquired from 1 mg/mL solution of **1** in dry CH_2Cl_2 containing 0.1 M TBAP as a supporting electrolyte. (b) Energy level diagram for P3HT, **1**−**3**, and PCBM.

LUMO = −3.3 eV) and PCBM (HOMO = −6.1 eV, LUMO = −3.9 eV) (Figure 3b).[4,19−23] If ZnFcs are located at the interface between P3HT and PCBM, ZnFcs can work as cosensitizers in the BHJ solar cells based on the P3HT/PCBM blended active layer. The cascaded energy levels of P3HT, ZnFcs, and PCBM at the BHJ interface may enable electrons and holes generated from ZnFc excitons to be injected into PCBM and P3HT, respectively. Figure 4a shows the UV−vis spectra of spin-coated films of P3HT/PCBM/**3** (in a 1:1:0.11 wt. ratio) before and after thermal annealing at 145 °C for 30 min. The as-cast film displayed a mixed absorption spectrum of P3HT and **3**, and the position of the Q-band agreed with that of **3** in the solution. After annealing, the absorbance of the P3HT band increased, and vibronic absorption shoulders appeared at a longer wavelength (500−620 nm), indicating the formation of an ordered stacking of P3HT backbones.[35] The thermal annealing of as-cast films leads to a formation of BHJ crystalline nanostructure by the phase separation of the blends, and the increased crystallinity enhances the carrier mobility and absorption coefficient of the P3HT/PCBM blended films.[36−38] The Q-band of **3** remained unaltered after the thermal annealing. ZnFc **3** was incorporated within the P3HT/PCBM blended film without the formation of aggregates. The other ZnFcs **1** and **2** in the blended films showed broad Q bands relative to **3**, suggesting the aggregation of ZnFcs.

BHJ solar cells were fabricated by using P3HT as the electron-donor materials and fullerene derivatives as the electron acceptor materials in the presence of ZnFcs **1**−**3** through the conventional spin-coating process. The cleaned tin-doped indium oxide (ITO)-coated glass anode was modified by spin-coating on poly(3,4-ethylenedioxythiophene)/polystyrene sulfonate (PEDOT/PSS) as a hole-extraction/electron-blocking layer with a 40 nm thickness. The active layer was deposited from the mixed chlorobenzene solutions onto the PEDOT/PSS-modified ITO anodes in an argon-filled glovebox ($[O_2]$ < 0.1 ppm and $[H_2O]$ < 0.1 ppm), and the thickness was typically 180 nm. After spin-coating, the resulting active layer was annealed at 145 °C for 10 min. TiO_x on the active layer has been used as an electron collection layer in the BHJ solar cells.[39] Finally, an aluminum cathode was deposited through a shadow mask by thermal evaporation under vacuum. Figure 4b

dx.doi.org/10.1021/am4005896 | ACS Appl. Mater. Interfaces 2013, 5, 4367−4373

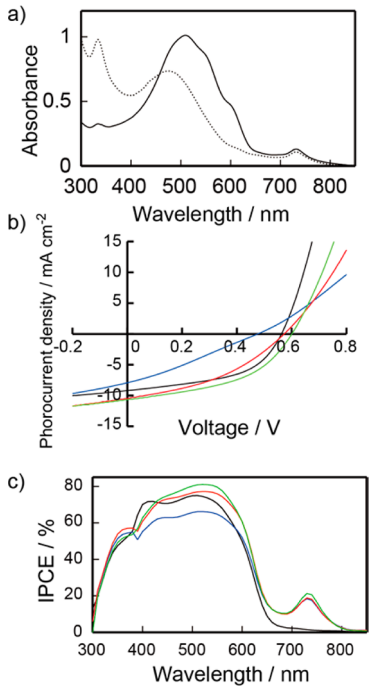

Figure 4. (a) UV−vis spectra of spin-coated films of P3HT/PCBM doped with **3** before (dotted line) and after annealing (solid line). (b) *J*−*V* curves of P3HT/PCBM blended films doped with **1** (blue line), **2** (red line), and **3** (green line) under a standard global AM 1.5 solar condition. The black line is the curve of the reference P3HT/PCBM cell without ZnFcs. (c) Incident photon-to-current conversion efficiency spectra for P3HT/PCBM blended films doped with **1** (blue line), **2** (red line), and **3** (green line). The black line is the spectrum of the reference P3HT/PCBM cell. The estimated J_{sc} values from the integration of IPCE spectra were almost agreed with the J_{sc} values obtained from *J*−*V* curves (The differences were less than 10%).

shows the *J*−*V* curves of BHJ solar cells fabricated from the mixed solution with a P3HT/PCBM/ZnFc composition with a weight ratio of 1:1:0.11 under a standard global AM 1.5 solar condition, and the device parameters (the short-circuit current density (J_{sc}), open-circuit voltage (V_{oc}), fill factor (FF), and overall power conversion efficiency (PCE)) of these cells are summarized in Table 1. The PCE of the cell with **3** was higher

Table 1. Summary of Device Performance for P3HT/PCBM Solar Cells Doped with 1−3[a]

	J_{sc} (mA cm^{-2})	V_{oc} (V)	FF	PCE (%)	R_{SA} (Ω cm^2)
P3HT/PCBM	−9.2	0.56	0.51	2.6	4.2
P3HT/PCBM/**1**	−7.9	0.49	0.28	1.1	28.8
P3HT/PCBM/**2**	−10.5	0.58	0.39	2.4	12.8
P3HT/PCBM/**3**	−10.7	0.60	0.46	3.0	7.1

[a]All parameters are averaged values for at least 8 devices.

than that of the control P3HT/PCBM cell, which was mainly due to the increase in J_{sc}. The addition of **3** increased J_{sc} by 1.5 mA cm^{-2} from 9.2 to 10.7 mA cm^{-2}. The PCE values were increased by increasing the dye concentration up to 5.4 wt % of **3**, and the device containing above 5.4 wt % of **3** showed a drop of PCE value. In contrast, the introduction of **1** and **2** decreased the PCE values, which can be ascribed to the formation of aggregates in the blended films. In particular, FF and the device series resistance (R_{SA}) strongly depended on the number of alkyl chains in ZnFcs.

The incident-photon to current conversion efficiency (IPCE) spectra of P3HT/PCBM BHJ solar cells doped with **1**−**3** were measured and compared with that of the reference P3HT/PCBM cell, as shown in Figure 4c. The IPCE spectra of BHJ solar cells with **1**−**3** exhibited an additional photocurrent at the ZnFcs absorption range, revealing that ZnFcs incorporated within P3HT/PCBM blended films effectively absorbed the incident light in the near-IR region and contributed to the photocurrent generation. While the IPCEs at 400−600 nm corresponding to the P3HT absorption were diminished by the addition of **1**, the cells with **2** and **3** exhibited improved IPCEs at this wavelength region. The dye contribution efficiency in the ternary blended BHJ solar cell with 5.2 wt % **3** is estimated to be 54% at 715 nm from the ration of the IPCE value to the absorption efficiency.[20] These results indicated that a majority of ZnFcs were located at the interface between P3HT and PCBM domains and acted as the mediator of charge transfer by the formation of energetic cascades. This observation agreed with the results of ternary blended BHJ solar cells cosensitized with MPcs.[19−23]

The surface morphologies of active layers with **1**−**3** were examined by tapping mode atomic force microscopy (AFM) to discuss the relationship between the solar cell performance and the film morphology (Figure 5). The samples were prepared by

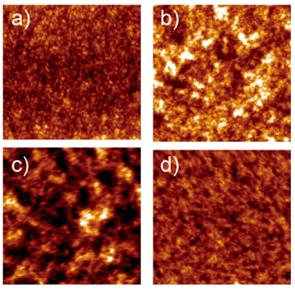

Figure 5. AFM images (5 × 5 μm) of P3HT/PCBM blended films without ZnFcs (a), doped with **1** (b), **2** (c), and **3** (d).

spin coating of a mixed solution on a quartz substrate, and the resulting thin films were annealed at 145 °C for 30 min. The P3HT/PCBM blended film exhibited a smooth surface composed of almost uniform sized island domains with a root-mean-square (rms) roughness of 2.31 nm. Although the blended film with **3** showed a similar domain size, the films with **1** or **2** contained larger sized domains as shown in Figure 5b and c. We found that the number of alkyl chains in the cosensitizers affected the phase-separation process of P3HT and PCBM, and **3** decorated with eight alkyl chains could disperse within the P3HT/PCBM blend films through van der Waals interaction among the alkyl chains. The AFM results are consistent with the corresponding solar cell performance. ZnFc **3** maintained the large interface area of the P3HT/PCBM active layer, and the morphology of nanoscale phase separation resulted in a better FF in the BHJ solar cell.

Photoinduced charge carrier mobility in the BHJ solar cells was measured by photoinduced charge carrier extraction in a linearly increasing voltage (Photo-CELIV) technique.[40] The Photo-CELIV current transient showed a single extraction peak at 2.5 μs caused by an applied offset bias at +0.15 V. The carrier mobility (μ) was estimated to be 1.8 × 10^{-4} cm^2 V^{-1} s^{-1},

dx.doi.org/10.1021/am4005896 | ACS Appl. Mater. Interfaces 2013, 5, 4367−4373

calculated by the equation reported by Mozer et al.[41] The obtained carrier mobility of our P3HT/PCBM cell was almost the same as the reported value.[40] In contrast, the charge carrier mobility of the cell doped with **3** ($\mu = 1.0 \times 10^{-4}$ cm^2 V^{-1} s^{-1}) was slightly low relative to that of the reference P3HT/PCBM cell. The low mobility may affect the FF value of the device performance.

CONCLUSION

In summary, we designed and synthesized new ring-expanded ZnFcs **1**−**3** fused with fluorene skeletons. Fusing fluorene rings with the porphyrazine rings resulted in a narrower band gap and stabilization of both the HOMO and LUMO energy levels compared with ZnPcs. We also demonstrated the expansion of the light-harvesting area in P3HT/PCBM BHJ solar cells by cosensitizing with ZnFcs. ZnFc **3** decorated with eight alkyl chains could disperse at the interface between P3HT and PCBM without unfavorable aggregation and contribute to the photocurrent generation by photoexcitation and enhancement of charge transfer between P3HT and PCBM. The incorporation of **3** at the interface of the BHJ structure of P3HT and PCBM lead to a higher device efficiency with 16% enhancement of J_{sc} as compared with that of the reference P3HT/PCBM BHJ solar cell. The systematic exploration of ring-expanded metallophthalocyanines may enhance the polymer-based BHJ solar cell performance by the expansion of the light harvesting area and the control of the phase-separation process.

EXPERIMENTAL SECTION

General. NMR spectra were recorded on a Bruker AVANCE 400 FT NMR spectrometer at 399.65 and 100.62 MHz for ^1H and ^{13}C in $CDCl_3$ solution. Chemical shifts are reported relative to internal TMS. IR spectra were obtained on a SHIMAZU IR Prestige-21 with DuraSample IR II. UV−vis spectra were measured on a JASCO V-650. MALDI-TOF mass spectra were obtained on a Bruker autoflex with dithranol as matrix. Atomic force microscopy images were acquired in noncontact mode by a JEOL JSPM-5400 system. The samples for AFM were prepared by the spin-coating of chlorobenzene solutions on glass substrate. Cyclic voltammetric measurements were recorded on an ALS 700 potentiostat using a three cell electrode system with a Pt working electrode, a Pt counter electrode and an Ag/AgCl reference electrode. TBAP was used as the electrolyte.

Materials. All chemicals were purchased from commercial suppliers and used without purification. P3HT was purchase from Aldrich (electronic grade) and used without any purification. Column chromatography was performed with silica gel (Wakogel C-200). Recycling preparative gel permeation chromatography was carried out by a JAI recycling preparative HPLC using $CHCl_3$ as an eluent. Analytical thin layer chromatography was performed with commercial Merck plates coated with silica gel 60 F_{254} or aluminum oxide 60 F_{254}. The purities of target compounds were confirmed by NMR, MALDI-TOF-Ms, and HPLC (purity was determined by the ratio between the peak area of compound and the total peak area).

Syntheses of Precursors. ***4***. A solution of $NaNO_2$ (0.63 g, 9.1 mmol) in water (10 mL) was added dropwise to a suspension of 3,4-dibromo-2-methylaniline (2 g, 7.6 mmol) in a mixture of water (60 mL) and 48% aqueous tetrafluoroboric acid (3.0 mL, 18.9 mmol) at 0 °C. The mixture was stirred at 0 °C for 1 h. After 1 h, the solution of potassium iodide (2.5 g, 0.015 mmol) in water (10 mL) was added to the mixture, and the reaction mixture was stirred at 0 °C for 1 h. The reaction mixture was poured into water, and the aqueous layer was extracted with 3 × 50 mL of Et_2O. The collected organic layer was washed with $Na_2S_2O_3$ and water. After the mixture was dried over Na_2SO_4, the solvent was evaporated and the residue was purified by column chromatography on silica gel by eluting with CH_2Cl_2 followed by recrystallization from methanol afforded **4** as white solid (1.9 g, yield 67%). ^1H NMR (400.13 MHz, $CDCl_3$): δ (ppm) 7.63 (d, J = 8.4 Hz, 1H, Ar*H*), 7.15 (d, J = 8.4 Hz, 1H, Ar*H*), 2.77 (s, 3H, −CH_3). ^{13}C NMR ($CDCl_3$, 100.61 Hz): δ (ppm) 142.9, 138.8, 132.2, 126.4, 126.2, 98.9, 31.6.

5. A solution of **4** (0.82 g, 2.2 mmol), 2-ethoxycarbonylphenylboronic acid pinacol ester (0.5 g, 1.8 mmol), and $Pd(PPh_3)_4$ (41.6 mg, 36 μmol) in toluene (6.6 mL), THF (8.3 mL), and 2 M K_2CO_3 aqueous solution (5 mL) was stirred at 70 °C for 48 h under nitrogen. After cooling to room temperature, the reaction mixture was poured into water, extracted with Et_2O. The organic layer was dried over Na_2SO_4 and solvent was evaporated. The residue was purified by column chromatography on silica using hexane/CH_2Cl_2 (10/1 v/v) and then (1/10 v/v) followed by recycling preparative HPLC to give **5** (0.74 g, yield 52%). ^1H NMR (400.13 MHz, $CDCl_3$): δ (ppm) 8.01 (d, J = 6.0 Hz, 1H, Ar*H*), 7.55 (t, J = 8.0 Hz, 1H, Ar*H*), 7.44−7.49 (m, 2H, Ar*H*), 7.17 (d, J = 8.0 Hz, 1H, Ar*H*), 6.91 (d, J = 8.4 Hz, 1H, Ar*H*), 4.04−4.12 (m, 2H, −COOCH_2-), 2.21 (s, 3H, −CH_3), 1.03 (t, J = 7.2 Hz, 3H, −CH_3). ^{13}C NMR ($CDCl_3$, 100.61 Hz): δ (ppm) 166.9, 142.2, 141.6, 138.5, 131.8, 130.6, 130.4, 130.3, 130.1, 128.5, 127.8, 127.3, 124.3, 60.9, 22.6, 13.7. IR (ATR): ν 1714 (−COO−) cm^{-1}.

6. A solution of **5** (0.74 g, 1.86 mmol) in concentrates sulfuric acid (22.3 mL) was stirred at room temperature for 12 h. The reaction mixture was poured into ice water, and it was stirred for a further 15 min. The aqueous layer was extracted with 3 × 50 mL of CH_2Cl_2. The solvent was evaporated, and the residue was purified by column chromatography on silica gel using CH_2Cl_2 to give **6** as yellow solid (0.63 g, 97%). ^1H NMR (400.13 MHz, $CDCl_3$): δ (ppm) 7.75 (s, 1H, Ar*H*), 7.73 (d, J = 6.8 Hz, 2H,Ar*H*), 7.53 (t, J = 7.6 Hz, 1H, Ar*H*) 7.35 (t, J = 7.2 Hz, 1H, Ar*H*), 2.80 (s, 3H, −CH_3). ^{13}C NMR ($CDCl_3$, 100.61 Hz): δ (ppm) 192.2, 144.6, 141.8, 136.5, 135.6, 135.4, 134.6, 134.3, 129.7, 126.8, 126.7, 125.1, 124.2, 21.9. IR (ATR): ν 1705 (−C═O) cm^{-1}.

7. The Grignard reagents were prepared from magnesium powders (100 mg, 4.1 mmol) in dry Et_2O (1 mL) and *p*-bromotoluene (8.2 mmol).Compound **6** (0.15 g, 0.43 mmol) was added into the Grignard solution and the resulted reaction mixture was refluxed for 12 h. The reaction mixture was hydrolyzed with saturated NH_4Cl solution followed by extracted with Et_2O.The organic layer was washed with water. The mixture was dried over $MgSO_4$ and the solvent was evaporated. The residue was purified by column chromatography on silica gel using CH_2Cl_2/hexane (1/10) and then (10/1) followed by recycling preparative HPLC to give **7** (0.16 g, 87%). ^1H NMR (400.13 MHz, $CDCl_3$): δ (ppm) 7.85 (d, J = 8.0 Hz, 1H, Ar*H*), 7.45 (s, 1H, Ar*H*), 7.40 (t, J = 6.8 Hz,1H, Ar*H*), 7.28−7.35 (m, 2H, Ar*H*), 7.22 (d, J = 8.4 Hz, 2H, Ar*H*), 7.09 (d, J = 8.4 Hz, 2H, Ar*H*), 2.92 (s, 3H, −CH_3), 2.39 (s, 1H, −O*H*), 2.31 (s, 3H, −CH_3). ^{13}C NMR ($CDCl_3$, 100.61 Hz): δ (ppm) 151.5, 151.3, 142.9, 139.9, 139.6, 138.2, 135.8, 129.7, 129.1, 128.8, 127.9, 125.6, 125.5, 124.0, 83.1, 21.8. IR (ATR): ν 3306 (−OH) cm^{-1}.

8. Compound **8** was synthesized from **6** and *p*-hexylphenyMgBr according to the same procedure of **7**. Yield: 69%. ^1H NMR (400.13 MHz, $CDCl_3$): δ (ppm) 7.85 (d, J = 7.6 Hz, 1H, Ar*H*), 7.46 (s, 1H, Ar*H*), 7.40 (t, J = 7.6 Hz, 1H, Ar*H*), 7.29−7.37 (m, 2H, Ar*H*), 7.23 (d, J = 8.4 Hz, 2H, Ar*H*), 7.08 (d, J = 8.4 Hz, 2H, Ar*H*), 2.92 (s, 3H, −CH_3), 2.40 (s, 1H, -O*H*), 1.53−1.61 (m, 2H, Ar−CH_2-), 1.24−1.35 (m, 8H, −CH_2−), 0.87 (t, J = 6.8 Hz, 3H, −CH_3). ^{13}C NMR ($CDCl_3$, 100.61 Hz): δ (ppm) 151.5, 151.3, 142.9, 139.9, 139.6, 138.2, 135.8, 129.7, 129.1, 128.8, 127.9, 125.6, 125.5, 124.0, 83.1, 36.0, 32.1, 31.7, 29.5, 23.0, 22.4, 14.5. IR (ATR): ν 3393 (−OH) cm^{-1}.

9. Compound **7** (0.41g, 0.92 mmol) was dissolved in dry toluene, and 0.16 mL CF_3SO_3H was added to this solution. The reaction mixture was heated at 50 °C with stirring for 10 min. The mixture was poured into an ice-cold $NaHCO_3$ aqueous solution. The product was extracted with Et_2O and the collected organic layer was dried over Na_2SO_4. After evaporation, the residue was purified by column chromatography on silica gel using CH_2Cl_2/hexane (1/1) to give diaryl compound as white solid (0.24 g, 50%). ^1H NMR (400.13 MHz, $CDCl_3$): δ (ppm) 7.93 (d, J = 7.6 Hz, 1H, Ar*H*), 7.51 (s, 1H, Ar*H*), 7.35−7.39 (m, 2H, Ar*H*), 7.29 (t, J = 7.6 Hz, 1H, Ar*H*), 7.03 (s, 8H, Ar*H*), 2.96 (s, 3H, −CH_3), 2.29 (s, 6H, −CH_3).

dx.doi.org/10.1021/am4005896 | ACS Appl. Mater. Interfaces 2013, 5, 4367−4373

A CuCN (290 mg, 3.3 mmol) was added to a solution of diaryl compound (240 mg, 0.41 mmol) in NMP (10 mL). After stirred at 180 °C for 24 h, the mixture was cooled down to room temperature, and 30% aqueous ammonia (30 mL) was added. The product was extracted with Et_2O and the collected organic layer was dried over Na_2SO_4. After evaporation, the residue was purified by column chromatography on silica gel using CH_2Cl_2/hexane (1/1) to give **9** as white solid (100 mg, 60%). ^{1}H NMR (400.13 MHz, $CDCl_3$): δ (ppm) 8.00 (d, J = 9.2 Hz, 1H, Ar*H*), 7.66 (s, 1H, Ar*H*), 7.48−7.40 (m, 3H, Ar*H*), 7.06 (d, J = 8.0 Hz, 4H, Ar*H*), 6.99 (d, J = 8.0 Hz, 4H, Ar*H*), 3.02 (s, 3H, −C*H*$_3$), 2.30 (s, 6H, −C*H*$_3$). ^{13}C NMR ($CDCl_3$, 100.61 MHz): δ 156.8, 152.9, 145.5, 143.5, 140.4, 138.6, 137.7, 137.41, 130.0, 129.4, 128.8, 128.2, 127.8, 126.6, 124.7, 116.4, 115.9, 115.3, 114.0, 65.1, 21.3, 20.9, 19.6. IR (ATR): ν 2337.72 (−CN) cm^{-1}.

10. Compound **10** was synthesized according to same procedure of **9**. Yield: 47% (for two steps). ^{1}H NMR (400.13 MHz, $CDCl_3$): δ (ppm) 8.00 (d, J = 9.6 Hz, 1H, Ar*H*), 7.66 (s, 1H, Ar*H*), 7.41−7.48 (m, 3H, Ar*H*), 7.03 (d, J = 6.0 Hz, 4H, Ar*H*), 6.98 (d, J = 6.0 Hz, 4H, Ar*H*), 3.02 (s, 3H, −C*H*$_3$), 2.55 (t, J = 7.6 Hz, 2H, ArC*H*$_2$-), 2.31 (s, 3H, −C*H*$_3$), 1.26−1.34 (m, 8H, −C*H*$_2$−), 0.87 (t, J = 6.8 Hz, 3H, −C*H*$_3$). ^{13}C NMR ($CDCl_3$, 100.61 MHz): δ 156.9, 152.9, 143.5, 142.4, 140.5, 138.5, 137.6, 137.4, 134.3, 130.0, 129.4, 128.9, 128.7,128.2, 127.8, 127.7, 126.6, 124.7, 116.4, 115.9, 115.3, 114.0, 65.1, 35.5, 31.7, 31.3, 29.0, 22.6, 20.9, 19.5, 14.1. IR (ATR): ν 2225.85 (−CN) cm^{-1}.

11. Compound **11** was synthesized from **8** with hexylbenzene and CH_3SO_3H. Yield: 12% (for two steps). ^{1}H NMR (400.13 MHz, $CDCl_3$): δ (ppm) 7.93 (d, J = 9.6 Hz, 1H, Ar*H*), 7.66 (s, 1H, Ar*H*), 7.44−7.49 (m, 3H, Ar*H*), 7.06 (d, J = 8.0 Hz, 4H, Ar*H*), 7.00 (d, J = 8.0 Hz, 4H, Ar*H*), 3.02 (s, 3H, −C*H*$_3$), 2.55 (t, J = 8.0 Hz, 4H, Ar C*H*$_2$−), 1.26−1.33 (m, 16H, −C*H*$_2$−), 0.87 (t, J = 8.0 Hz, 6H, −C*H*$_3$). ^{13}C NMR ($CDCl_3$, 100.61 MHz): δ 157.3, 153.4, 143.9, 142.9, 141.0, 138.9, 138.1, 130.3, 129.3, 129.1, 128.6, 128.2, 127.1, 125.1, 116.85, 116.3, 115.7, 114.4, 65.5, 35.9, 32.1, 31.7, 29.5, 23.0, 20.0, 14.4. IR (ATR): ν 2223.92 (−CN) cm^{-1}.

*Zinc Fluorecyanines **1**−**3***. ***1***. A mixture of **9** (200 mg, 296 μmol) and $Zn(CH_3COO)_2$ (43 mg, 197 μmol) in 4 mL of DMAE was heated at 150 °C with stirring for 24 h. After the mixture was cooled, the solvent was removed and washed with methanol several time to remove excess Zn ion. The residue was purified by column chromatography on activated alumina by eluting with CH_2Cl_2 and recycling preparative HPLC to give **1**. Yield: 36 mg, 35%. ^{1}H NMR ($CDCl_3$, 400.13 MHz): δ (ppm) 9.28−9.36 (m, 4H, Ar*H*), 8.53−8.56 (m, 4H, Ar*H*), 7.58−7.67 (m, 8H, Ar*H*), 7.41−7.58 (m, 20H, Ar*H*), 7.13−7.18 (m, 16H, Ar*H*), 4.43−4.54 (m, 12H, −C*H*$_3$), 2.34 (s, 24H, −C*H*$_3$). MALDI-TOF Ms (dithranol): m/z 1705 (M + H). Calcd for $C_{120}H_{88}N_8Zn$: m/z 1705.6.

ZnFcs **2** and **3** were synthesized by the same procedure of **1**.

2. Yield: 26%. ^{1}H NMR ($CDCl_3$, 400.13 MHz): δ (ppm) 9.34−9.36 (m, 4H, Ar*H*), 8.55−8.57 (m, 4H, Ar*H*), 7.58−7.69 (m, 8H, Ar*H*), 7.42−7.51 (m, 20H, Ar*H*), 7.15−7.19 (m, 16H, Ar*H*), 4.44−4.56 (m, 12H, −C*H*$_3$), 2.57 (br, 8H, ArC*H*$_2$-), 2.34 (s, 24H, −C*H*$_3$), 1.60 (br, 8H, −C*H*$_2$−), 1.25−1.31 (m, 24H, −C*H*$_2$), 0.82 (t, 12H, −C*H*$_3$). MALDI-TOF Ms (dithranol): m/z 1987 (M + H). Calcd for $C_{140}H_{128}N_8Zn$: m/z 1985.9.

3. Yield: 49%. ^{1}H NMR ($CDCl_3$, 400.13 MHz): δ (ppm) 9.36−9.40 (m, 4H, Ar*H*), 8.54−8.56 (m, 4H, Ar*H*), 7.57−7.68 (m, 8H, Ar*H*), 7.41−7.49 (m, 20H, Ar*H*), 7.14−7.18 (m, 16H, Ar*H*), 4.43−4.55 (m, 12H, −C*H*$_3$), 2.57 (br, 16H, ArC*H*$_2$−), 1.59 (br, 16H, −C*H*$_2$−), 1.24−1.30 (m, 48H, −C*H*$_2$), 0.83 (t, 24H, −C*H*$_3$). MALDI-TOF Ms (dithranol): m/z 2265 (M + H). Calcd for $C_{160}H_{168}N_8Zn$: m/z 2265.2.

Fabrication of BHJ Solar Cells. Indium tin oxide (ITO) patterned glass substrates were cleaning with sonication in neutral detergent, distilled water, acetone, and 2-propanol. The substrates were dried and apply UV−O_3 treatment for 30 min. Electron blocking layer were prepared by spin-coated the PEDOT/PSS (H. C. Starck) with a thickness of 40 nm. The substrates were baked at 200 °C for 10 min under an ambient condition. A solution containing a mixture of P3HT, PCBM, and ZnFcs (1:1:0.11 wt. ratio) in chlorobenzene were spin-coated onto the PEDOT/PSS layer and apply thermal annealing treatment at 150 °C for 10 min in the argon filled globe box. Titanium oxide solution was spin-coated onto the active layer then place in air for 30 min. The counter electrode of aluminum was prepared by thermal deposition with a thickness of 100 nm. Current density−voltage (J−V) characteristics were measured using a Keithley 2400 Source Measure Unit. Performance of BHJ solar cells devices was measured under one-sun conditions (AM 1.5, 100 mW cm^{-2}) by a solar simulator (XES-151S, Sanei Electric, Inc.).

AUTHOR INFORMATION

Corresponding Author

*E-mail: mkimura@shinshu-u.ac.jp.

Notes

The authors declare no competing financial interest.

ACKNOWLEDGMENTS

This work has been partially supported by Grants-in-Aid for Scientific Research (B) (No. 22350086) from Japan Society for the Promotion of Science (JSPS) and the New Energy and Industrial Technology Development Organization (NEDO) of Japan. The authors thank Prof. Shogo Mori and Koichi Okuda of Shinshu University for the analyses of Photo-CELIV.

REFERENCES

(1) Günes, S.; Neugebauer, H.; Sariciftci, N. S. *Chem. Rev.* **2007**, *107*, 1324−1338.

(2) Cheng, Y.-J.; Yang, S.-H.; Hsu, C.-S. *Chem. Rev.* **2009**, *109*, 5868−5923.

(3) Brabec, C. J.; Gowrisanker, S.; Halls, J. J. M.; Laird, D.; Jia, S.; Williams, S. P. *Adv. Mater.* **2010**, *22*, 3839−3856.

(4) Shaheen, S. E.; Brabec, C. J.; Sariciftci, N. S.; Padingger, F.; Fromherz, T.; Hummelen, J. C. *Appl. Phys. Lett.* **2001**, *78*, 841.

(5) Clarke, T. M.; Durrant, J. R. *Chem. Rev.* **2010**, *110*, 6736−6767.

(6) Rivnay, J.; Mannsfeld, S. C. B.; Miller, C. E.; Salleo, A.; Toney, M. F. *Chem. Rev.* **2012**, *112*, 5488−5519.

(7) Schilinsky, P.; Waldauf, C.; Brabec, C. J. *Appl. Phys. Lett.* **2002**, *81*, 3885.

(8) Reyes-Reyes, M.; Kim, K.; Carroll, D. L. *Appl. Phys. Lett.* **2005**, *87*, No. 083506.

(9) Li, G.; Shrotriya, V.; Huang, J.; Yao, Y.; Moriarty, T.; Emery, K.; Yang, Y. *Nat. Mater.* **2005**, *4*, 864−868.

(10) Kim, Y.; Cook, S.; Tuladhar, S. M.; Choulis, S. A.; Nelson, J.; Durrant, J. R.; Bradley, D. D. C.; Giles, M.; McCulloch, I.; Ha, C.-S.; Ree, M. *Nat. Mater.* **2006**, *5*, 197−203.

(11) Hoth, C. N.; Choulis, S. A.; Schilinsky, P.; Brabec, C. J. *Adv. Mater.* **2007**, *19*, 3973−3978.

(12) Lobez, J. M.; Andrew, T. L.; Bulović, V.; Swager, T. M. *ACS. Nano* **2012**, *6*, 3044−3056.

(13) Neugebauer, H.; Loi, M. A.; Winder, C.; Sariciftci, N. S.; Cerullo, G.; Gouloumis, A.; Vázquez, P.; Torres, T. *Sol. Energy Mater. Sol. Cells* **2004**, *83*, 201−209.

(14) Johansson, E. M. J.; Yartsev, A.; Rensmo, H.; Sundström, V. *J. Phys. Chem. C* **2009**, *113*, 3014−3020.

(15) Peet, J.; Tamayo, A. B.; Dang, X.-D.; Seo, J. H.; Nguyen, T.-Q. *Appl. Phys. Lett.* **2008**, *93*, 163306.

(16) Suresh, P.; Balraju, P.; Sharma, G. D.; Mikroyannidis, J. A.; Stylianakis, M. M. *Appl. Mater. Interface* **2009**, *1*, 1370−1374.

(17) Sharma, S. S.; Sharma, G. D.; Mikroyannidis, J. A. *Sol. Energy Mater. Sol. Cells* **2011**, *95*, 1219−1223.

(18) de la Torre, G.; Claessens, C. G.; Torres, T. *Chem. Commun.* **2007**, 2000−2015.

(19) Honda, S.; Nogami, T.; Ohkita, H.; Benten, H.; Ito, S. *Appl. Mater. Interface* **2009**, *1*, 804−810.

(20) Honda, S.; Ohkita, H.; Benten, H.; Ito, S. *Chem. Commun.* **2010**, *46*, 6596−6598.

(21) Honda, S.; Ohkita, H.; Benten, H.; Ito, S. *Adv. Energy Mater.* **2011**, *1*, 588−598.

(22) Hori, T.; Masuda, T.; Fukuoka, N.; Hayashi, T.; Miyake, Y.; Kamikado, T.; Yoshida, H.; Fujii, A.; Shimizu, Y.; Ozaki, M. *Org. Electron.* **2012**, *13*, 335−340.
(23) Lee, J. U.; Kim, Y. D.; Jo, J. W.; Kim, J. P.; Jo, W. H. *J. Mater. Chem.* **2011**, *21*, 17209−17218.
(24) Mack, J.; Kobayashi, N. *Chem. Rev.* **2011**, *111*, 281−321.
(25) Kobayashi, N.; Furuyama, T.; Satoh, K. *J. Am. Chem. Soc.* **2011**, *133*, 19642−19645.
(26) Muranaka, A.; Yonehara, M.; Uchiyama, M. *J. Am. Chem. Soc.* **2010**, *132*, 7844−7845.
(27) Li, C.; Liu, M.; Pschierer, N. G.; Baumgarten, M.; Müllen, K. *Chem. Rev.* **2010**, *110*, 6817−6855.
(28) Kajigaeshi, S.; Kakinami, T.; Tokiyama, H.; Hirakawa, T.; Okamoto, T. *Chem. Lett.* **1987**, 627−630.
(29) Diemer, V.; Leroux, F. R.; Colobert, F. *Eur. J. Org. Chem.* **2011**, 327−340.
(30) Hussain, I.; Yawer, M. A.; Lau, M.; Pundt, T.; Fischer, C.; Görls, Langer, P. *Eur. J. Org. Chem.* **2008**, 503−518.
(31) Wong, K.-T.; Wang, Z.-J.; Chien, Y.-Y.; Wang, C.-L. *Org. Lett.* **2001**, *3*, 2285−2288.
(32) Stillman, M. J.; Nyokong, T. *Phthalocyanines Properties and Applications*, Vol. *1*; Leznoff, C. C., Lever, A. B. P., Eds.; VCH: New York, 1989; Chapter 3, pp 139−247.
(33) Lever, A. B. P.; Milaeva, E. R.; Speier, G. *Phthalocyanines Properties and Applications*, Vol. 3; Leznoff, C. C., Lever, A. B. P., Eds.; VCH: New York, 1993; Chapter 1, pp 1−70.
(34) Grisorio, R.; Allegretta, G.; Suranna, G. P.; Mastrorilli, P.; Loiudice, A.; Rizzo, A.; Mazzeo, M.; Gigli, G. *J. Mater. Chem.* **2012**, *22*, 19752−19760.
(35) Samitsu, S.; Shimomura, T.; Heike, S.; Hashizume, T.; Ito, K. *Macromolecules* **2008**, *41*, 8000−8010.
(36) Padinger, F.; Rittberger, R. S.; Sariciftci, N. S. *Adv. Funct. Mater.* **2003**, *13*, 85−88.
(37) Moulé, A. J.; Allard, S.; Kronenberg, N. M.; Tsami, A.; Scherf, U.; Meerholz, K. *J. Phys. Chem. C* **2008**, *112*, 12583−12589.
(38) Ma, W.; Yang, C.; Gong, X.; Lee, K.; Heeger, A. J. *Adv. Funct. Mater.* **2005**, *15*, 1617−1622.
(39) Hayakawa, A.; Yoshiokawa, O.; Fujieda, T.; Uehara, K.; Yoshikawa, S. *Appl. Phys. Lett.* **2007**, *90*, No. 163517.
(40) Mozer, A. J.; Sariciftci, N. S.; Lutsen, L.; Vanderzande, D.; Österbacka, R.; Westerling, M.; Juška, G. *Appl. Phys. Lett.* **2005**, *86*, No. 112104.
(41) De Villers, B. T.; Tassone, C. J.; Tolbert, S. H.; Schwartz, B. J. *J. Phys. Chem. C* **2009**, *113*, 18978−18982.